Supplemental Document

Direct measurement of individual optical forces in ensembles of trapped particles: supplement

FRANZISKA STRASSER, SIMON MOSER, MONIKA RITSCH-MARTE, AND GREGOR THALHAMMER*

Medical University of Innsbruck, Institute of Biomedical Physics, Müllerstraße 44, 6020 Innsbruck, Austria
**Corresponding author:* *gregor.thalhammer@i-med.ac.at*

Supplement DOI: https://doi.org/10.6084/m9.figshare.13417403

Parent Article DOI: https://doi.org/10.1364/OPTICA.410494

Direct measurement of individual optical forces in an ensemble of trapped particles: supplemental document

1. ALGORITHM FOR LIGHT FIELD PROPAGATION

In this section we discuss the algorithm used for the propagation between the different planes in more detail. The algorithm, which is based on the on Collins integral [1], can be rewritten as a convolution with additional phase factors. It can be expressed by Fourier transforms

$$E_2(\mathbf{r}_2) \propto e^{\frac{-i\pi}{\lambda B}(D-1)r_2^2}\mathcal{F}^{-1}\left[\mathcal{F}\left(E_1(\mathbf{r}_1)e^{-i\frac{\pi}{\lambda B}(A-1)r_1^2}\right)\mathcal{F}\left(e^{-i\frac{\pi}{\lambda B}r_1^2}\right)\right] \tag{S1}$$

or more concisely as

$$E_2 = \mathcal{P}(E_1) = \omega_2\mathcal{F}^{-1}\left[\mathcal{F}(E_1\omega_1)\mathcal{F}(\omega_{12})\right]. \tag{S2}$$

Here A,B,D are elements of the ABCD or ray transfer matrix describing the optical system between planes with optical fields $E_1(\mathbf{r}_1)$ and $E_2(\mathbf{r}_2)$ in the paraxial approximation. We have omitted global phase and scaling factors.

The corresponding inverse propagation is needed for gradient backpropagation in the gradient based optimization procedure, see Sec. 2.C.4. in the main text. It is given by

$$\bar{E}_1 = \mathcal{P}^{-1}(\bar{E}_2) = \omega_1^*\mathcal{F}^{-1}\left[\mathcal{F}(\bar{E}_2\omega_2^*)\mathcal{F}(\omega_{12}^*)\right], \tag{S3}$$

which has a very similar structure as the forward propagator $\mathcal{P}$ in Eq. S3, but with planes 1 and 2 exchanged, and the phase factors ω_i are replaced by their complex conjugate ω_i^*.

This propagation algorithm is based on the Fresnel approximation of the Kirchhoff diffraction integral. As such it does not reflect the vectorial nature of light, which can have significant deviations close to the focus of high-NA optics compared to scalar approximation. Using a more rigorous but computationally more expensive vectorial propagation method [2] turned out to be not needed: polarization effects with our samples are negligibly small, therefore it is enough to consider only a single polarization component. Furthermore, since we use the same scalar propagation method to calculate both the field in the object plane from the incoming field in the pupil plane, and also to calculate the back focal plane field from the object plane field, in total the errors cancel and the far-field resembles the physical truth well. The fields obtained for the object plane are actually not correct, but since we only use the localization property of the field in the object plane, which both methods provide in similar manner, this approximation is well justified, and it helps to speed up the computations significantly.

2. CORRECTION OF CONDENSER DISTORTION

In this section we give a detailed description of our procedure to characterize and compensate the distortions of the condenser lens present in the BFP image. We display a calibration pattern consisting of a regular rectangular grid of 16×16 points on the SLM. From the measured positions of the corresponding spots in the BFP image we

calculate the coefficients of a general 2D polynomial of order 4 that relates the positions of the spot positions to the undistorted grid, minimizing the total least-square difference between measured and estimated position. Due to the limited numerical aperture (NA) of the objective lens of 1.2, which is smaller than the maximum possible value of NA=1.33 that can be transmitted for a water filled sample chamber, this calibration procedure misses support grid points at the border. Here we rely on extrapolation by the polynomial.

Based on this polynomial approximation we calculate an undistorted BFP image. For each pixel in the resulting image we take the linearly interpolated intensity of the measured, distorted image at the corresponding position. With this procedure the remaining misalignment between a corrected BFP image and a numerically propagated SLM patterns is typically less than one SLM pixel (SLM size 512×512 pixels).

3. DETAILED OPTICAL SETUP

Here we show the full optical setup (see Fig. S1) and list the used optical elements and other devices in Table S1.

The achromatic doublet lenses L3 and L4, which image the SLM surface onto the back focal plane of the objective lens, need to be aligned with care. The distances of the lenses must be set such that a $4f$ relay optics configuration is fulfilled, otherwise off-axis beams are clipped at the aperture of the objective lens. Furthermore, the orientation of the achromatic doublets is chosen such that the weakly curved surface of lens L3 points towards the SLM, and for lens L4 the weakly curved surface is pointing towards the objective lens. This configuration provides the best imaging quality from the SLM plane to the pupil plane.

To improve the imaging of the inclined SLM surface to the pupil plane of the objective lens, which is oriented orthogonal to the optical axis, the lenses L3 and L4 are slightly tilted. We used the software Zemax OpticsStudio to find an optimal configuration, which is given as a compromise between aberrations induced by tilting the lenses, and inclination of the image plane with respect to the pupil plane. The polarization

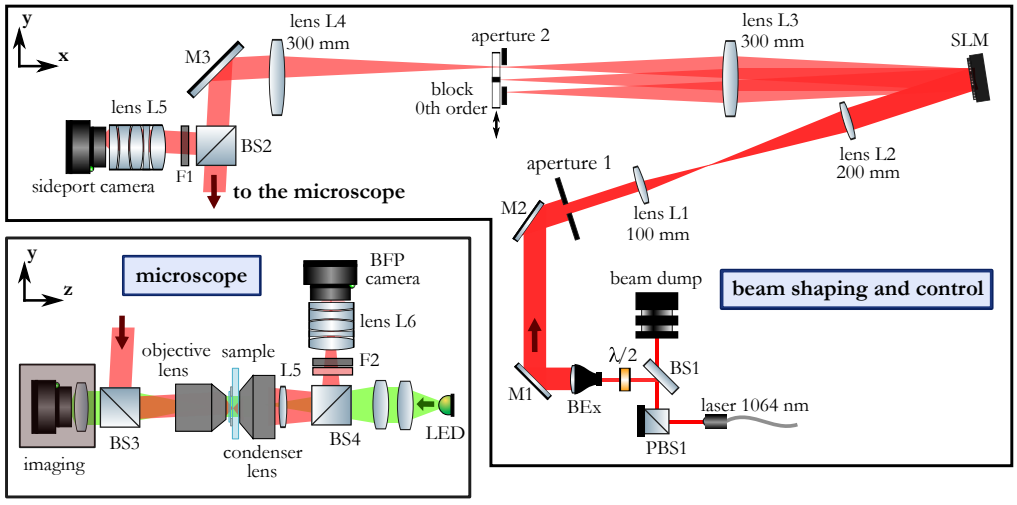

Fig. S1. Schematic drawing of our holographic optical tweezers setup. For details about the optical elements and devices see Table S1. The setup is split up into two parts. The first part is used to control and shape the laser beam. The second part consists of the inverted upright microscope where the trapping takes place and the main cameras for imaging the back focal plane and the sample are located. The block for the 0th order of the SLM is mounted in a flip mount.

Table S1. Detailed description of parts use for the optical setup shown in Fig.S1.

Laser	fiber laser, max. power 10 W, wavelength 1064 nm (IPG, PLY-10-1064-LP)
PBS1	polarizing beamsplitter, size 13 mm
BS1	beam sampler, fused silica, back-side with anti-reflective coating, diameter 25 mm (Thorlabs BSF10-B)
$\lambda/2$	half-wave plate, wavelength 1064 nm, diameter 13 mm
BEx	2× beam expander (Thorlabs BE02M)
M1/M2	dielectric mirror, diameter 25 mm (Thorlabs BB1-E03)
L1	achromatic doublet lens, focal length 100 mm, diameter 25 mm (Thorlabs AC254-100-B)
L2/L5	achromatic doublet lens, focal length 200 mm, diameter 25 mm (Thorlabs AC254-200-B)
SLM	LCoS spatial light modulator, resolution 512×512, wavelength 1064 nm (Meadowlark Optics HSPDM512-1064)
L3/L4	achromatic doublet lens, focal length 300 mm, diameter 51 mm (Thorlabs AC508-300-B)
M3	dielectric mirror, diameter 51 mm, thickness 10 mm (EKSMA Optics BK7 flat harmonic separator, HR>99% at 1064 nm, HT>97% at 532 nm, AOI = 45°)
BS2	non-polarizing beamsplitter, 10/90 (R/T), size 20 mm (Thorlabs BS044)
F1	stack of absorptive neutral density filters, transmission $\sim 10^{-4}$, diameter 25 mm (Thorlabs ND10B, ND30B)
L5/L6	camera lens, focal length 50 mm, aperture 1:2.8, diameter 30.5 mm (Tamron 23FM50SP)
side port/imaging camera	CMOS monochrome camera, sensor Sony IMX174, resolution 1920×1200 (Matrix Vision, mvBlueFOX3-2024-G)
BS3/BS4	non-polarizing beamsplitter, 50/50 (R/T), size 25 mm (Thorlabs BS014)
objective lens	water-immersion objective lens, 60×, NA 1.2 (Olympus UPLSAPO60XW)
condenser lens	achromatic aplanatic condenser lens, NA 1.35, oil immersion (Nikon Achromat Aplanatic Condenser)
F2	stack of 850 nm longpass filter (Thorlabs FGL850M) and absorptive neutral density filters, transmission $\sim 10^{-3}$, diameter 25 mm (typically Thorlabs ND10B and ND20B)
BFP camera	CMOS camera, resolution 1280×1024, sensor ON Semiconductor PYTHON 1300, NIR enhanced (Ximea MQ013RG-ON)

direction of the trapping light is aligned horizontally, which after reflection at mirror M3 and BS3 translates to a linear polarization in the sample chamber aligned with the x-direction (left-right direction in the particle images of Figs. 3–7 of the main text). To minimize unwanted polarization effects the SLM head is mounted such that its alignment direction is also horizontal, within the plane of the in- and outgoing laser beams.

4. ENHANCED METHOD FOR MEASURING ANGULAR INTENSITY DISTRIBUTION OF INGOING TRAPPING LIGHT

In order to accurately determine the intensity distribution of the trapping laser at the SLM surface without contributions from unwanted reflections at the SLM surface, we display blazed grating patterns on the SLM to divert the light and block the unwanted reflections with a metal stripe in the intermediate focal plane, masking out light close to the optical axis. The intensity modulations at the phase wrapping lines are removed in a post processing step by averaging with a median filter over several patterns with gratings oriented at different angles. This approach also reduces distortions induced by dust particles present in the optical train and the probe chamber. As the beam direction is altered by changing the grating orientation, the diffraction patterns of dust change position and are effectively removed by averaging.

The total power in the intensity distribution measured by this procedure lies below the actual one at the SLM due to limited diffraction efficiency. Hence, we rescale the intensity according to our model calculation of the SLM diffraction efficiency. Furthermore, we account for the non-uniform, angle-dependent light losses induced by the sample chamber and condenser lens by dividing the intensity by the transmission function T. This procedure yields the far-field intensity distribution of the incoming light for a uniform pattern, which we use as the illumination for the SLM in our retrieval, assuming no additional angle-dependent losses, e.g., in the objective lens.

5. ESTIMATION OF THE INCOMING AXIAL MOMENTUM FLUX FOR DIRECT FORCE MEASUREMENTS

The reconstructed individual light fields provide us with information about the *outgoing* momentum flux $\mathbf{F}_{\text{out}}$ of the trapping light. Due to momentum conservation the exerted force $\mathbf{F}$ is given as the difference of the incoming momentum flux $\mathbf{F}_0$

$$\mathbf{F} = \mathbf{F}_{\text{out}} - \mathbf{F}_0. \tag{S4}$$

To obtain knowledge about the exerted force one also needs information about $\mathbf{F}_0$. This is an issue mostly for the axial force component, because there is a large momentum flux along the beam direction, whereas the radial components of $\mathbf{F}_0$ can be easily adjusted to zero by aligning the trapping laser beam to be centered around the optical axis.

Depending on the experimental settings one has to choose an adequate approach to determine $\mathbf{F}_0$. Generally we prefer to use our detection scheme for $\mathbf{F}_{\text{out}}$ to also obtain consistent data for $\mathbf{F}_0$. Repeating experiments with empty traps, where the ingoing light is transmitted unaffectedly, reveals changes to $\mathbf{F}_0$ induced, e.g., by different phase patterns used to steer trap positions. Alternatively $\mathbf{F}_0$ can be calculated from the known amplitude (see also Sec. 4) and the phase pattern displayed at the SLM, as discussed in Sec. 4.A of the main text. This avoids repeating the experiment, but it is more sensitive to a mismatch of the model with the actual settings.

For trapped particles in a static configuration a simple approach is to employ that in equilibrium the mean exerted force $\langle \mathbf{F} \rangle$ is zero (provided that external forces such as drag forces due to a fluid flow are absent). Consequently one can set $\mathbf{F}_0$ to the mean value $\langle \mathbf{F}_{\text{out}} \rangle$ of the observed momentum flux.

A. Estimation of F_0 in the presence of laser noise

In the presence of dynamic fluctuations that influence the ingoing momentum flux[1] F_0, such as laser intensity noise, the above approaches to estimate F_0 cannot be used. Either we rely on the assumption of static conditions, or that repeating an experiment with empty traps uses precisely the same F_0. The latter assumption is not fulfilled for the data presented in Sec. 4.B.2, where we study the forces related to the thermal motion. In this experiment the forces are so weak that laser intensity noise needs to be taken into account. Since the incoming flux $F_0 \propto P$ is proportional to the total laser power P, fluctuations ΔP of the power $P = \langle P \rangle + \Delta P$ around its mean value $\langle P \rangle$ will affect F_{out}, which can be described by

$$F_{\text{out}} = F + \langle F_0 \rangle \frac{P}{\langle P \rangle} = F + \langle F_0 \rangle \left(1 + \frac{\Delta P}{\langle P \rangle}\right). \tag{S5}$$

The axial component of the incoming momentum flux F_0 is particularly large, about 100 times larger than the typical force due to thermal motion in our experiment. In this case the amount of noise originating from the power fluctuations is similar to the force signal of the thermal motion and needs to be compensated.

Since we work with weakly scattering particles, the incoming power of each trapping beam is hardly changed. Due to the small excursion of the particles in the thermal force measurements this is maintained at a largely constant level. Even if some fraction of the light is lost, we have $\frac{P}{\langle P \rangle} \approx \frac{P_{\text{out}}}{\langle P_{\text{out}} \rangle}$ well fulfilled. With this and using the above mentioned fact that for a trapped particle in equilibrium the mean exerted force is zero and consequently $\langle F_{\text{out}} \rangle = \langle F_0 \rangle$, we can estimate the incoming momentum flux by $F_0 \approx \langle F_{\text{out}} \rangle \frac{P_{\text{out}}}{\langle P_{\text{out}} \rangle}$, only using measurements of the outgoing momentum flux and power.

When analyzing the experiment for the thermal force characterization we rely on the theory for the stochastic motion $x(t)$ of a trapped particle. We rewrite it in terms of the optical force, where we assume a linear relationship $F = -\kappa x$ between force and position, with κ denoting the trap stiffness. The trap stiffness also scales with trap power, $\kappa = \langle \kappa \rangle \frac{P}{\langle P \rangle}$, and we get

$$F_{\text{out}} = \big(-\langle \kappa \rangle x + \langle F_0 \rangle \big) \frac{P}{\langle P \rangle}. \tag{S6}$$

This reveals that by dividing F_{out} by the (normalized) power, which is well approximated by $\frac{P}{\langle P \rangle} \approx \frac{P_{\text{out}}}{\langle P_{\text{out}} \rangle}$ as stated above, we are able to compensate for the power fluctuations and recover the forces due to thermal motion. Depending on the specific interest for a measurement, one may choose $-\kappa x$ or $-\langle \kappa \rangle x$ as an estimate for the "true" thermal force in the presence of laser noise. Anyhow, the relative difference is $\frac{\Delta P}{P}$, which is on the order of 1 % in our setup.

As said above, for the radial direction, F_0 is close to zero for a trapping laser well centered on the optical axis and compensation for F_0 is not needed. We observe no signficant difference if we apply the normalization for the radial directions.

B. Compensation of model imperfections by enforcing energy conservation

The above described approach to compensate for laser noise relies, among other things, on the fact that in our settings with particles of relatively low refractive index (silica microspheres, red blood cells) scattering is weak and the ingoing and outgoing laser power have a fixed ratio. As this is not generally true, this relation is not enforced in our field retrieval algorithm. This leaves the algorithm the freedom to alter the power of one or more traps to match the observed data by the model calculations. If we have

[1] We note that here we only consider the axial force component, but the theoretical considerations given below apply to the force component in any direction.

imperfections in our model this can introduce errors in the estimates of the power of the individual trapping beams. As described in Sec. 4.A of the main text, a simple way to enforce energy conservation is to divide the obtained individual force F_{out} by P/P_0, similar to the approach above. Here P_0 is the *expected* in- and outgoing power, which is either estimated or measured by repeating the experiment using a single trap. Again, this we perform only for the axial force component.

6. INDEPENDENCE OF RETRIEVED INDIVIDUAL FORCES

The good agreement between the retrieved individual forces and the expected value, as shown in the main text for 10 microspheres (see Sec. 4.A and Fig. 7) supports our finding that our method provides sufficiently independent measurements of the individual forces. For these results we compared the retrieved individual forces with single-trap measurements, where we repeated the trap movements one by one. However, drifts or fluctuations of beam position, microscope stage position, or laser power between the measurements can induce deviations that should not be attributed to our method.

Here we present simultaneous measurements with four traps (plus one reference trap), where two traps are left empty. The two active traps are scanned over two fixed microspheres by changing the phase pattern on the SLM. They paths follow different directions, along the x- and y-axis respectively. The retrieved forces for the two empty traps, which stay at fixed positions, are expected to be zero, independent of the exact beam placement. This allows a more reliable comparison of the individual retrieved forces with the expected value of zero.

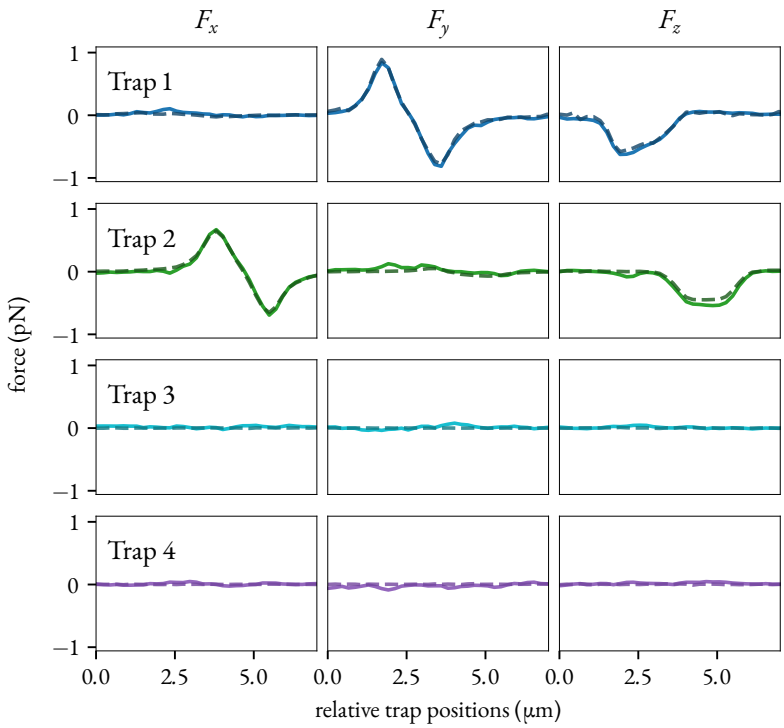

Fig. S2. Individual force profiles obtained from simultaneous measurements with 4 traps (solid lines) and single-trap measurements (dashed lines). Trap 1 and 2 are scanned over silica microspheres in directions x and y, respectively, with different offsets to their center. Trap 3 and 4 pass the sample unobstructed and are not moved throughout the measurement.

In Fig. S2 all components of the individual forces for the four traps are shown. It also contains the result for the corresponding single-trap measurements. This data was rescaled according to the calculated ratio of the power in the individual spots for single- und multi-trap measurements. In general we observe good agreement between the individual retrieved forces and the single-trap reference data. For the empty traps (trap 3 and 4) some deviations from the expected value of zero are visible. No clear similarity with the force profiles of the occupied traps is visible. The root mean square force amounts to 0.025 pN, which is about 3% of the maximal exerted force of 0.84 pN for these particles. Compared to the ingoing axial momentum flux $F_{0,z} = 7$ pN, which defines the scale for the maximally possible optical force, the observed mean deviation is only 0.4 %. This measurement confirms our expectations from the 10 traps measurement that our method provides accurate results for the individual forces, with errors in the few-percent range.

REFERENCES

1. S. A. Collins, "Lens-system diffraction integral written in terms of matrix optics*," J. Opt. Soc. Am. A **60**, 1168–1177 (1970).
2. B. Boruah and M. Neil, "Focal field computation of an arbitrarily polarized beam using fast Fourier transforms," Opt. Commun. **282**, 4660–4667 (2009).